SciEn

Proceedings of 8th International Conference on Mechanical Engineering and Renewable Energy 2025
10-12 December, 2025, Chattogram, BANGLADESH

SciEn Conference Series: Engineering Vol. 4, 2026, pp 507-513 https://doi.org/10.38032/scse.2026.4.224

Effect of Strontium Dopant on Dielectric Properties of $BaTiO_3$

Md Asif Shahriar[1,2], Md Mahfuzul Haque[1], Md. Mostafizur Rahman Suruj[2,3] and Md Miftaur Rahman[1]

[1]Department of Materials and Metallurgy Engineering, Bangladesh University of Engineering and Technology (BUET), Dhaka- 1000, Bangladesh
[2]Department of Nanomaterials and Ceramic Engineering, Bangladesh University of Engineering and Technology (BUET), Dhaka- 1000, Bangladesh
[3]Department of Ceramic and Metallurgy Engineering, Rajshahi University of Engineering and Technology, Rajshahi-6204, Bangladesh

ABSTRACT

Strontium-doped barium titanate ($Ba_{1-x}Sr_xTiO_3$, BST) ceramics with Sr concentrations of 1%, 3%, and 5% were successfully synthesized using the conventional solid-state reaction method. High-purity barium carbonate ($BaCO_3$), strontium carbonate ($SrCO_3$), and titanium dioxide (TiO_2) powders were thoroughly mixed and milled for 24 hours, followed by pellet formation and sintering at 1150–1250 °C for 2 hours. The phase composition, microstructure, and dielectric properties of the samples were systematically investigated. X-ray diffraction (XRD) confirmed the formation of a single-phase perovskite structure, with a tetragonal-to-cubic phase transition observed as Sr content increased. The lattice parameters decreased with Sr incorporation due to the smaller ionic radius of Sr^{2+} (1.16 Å) compared to Ba^{2+} (1.36 Å), confirming successful A-site substitution. The dielectric constant increased from pure $BaTiO_3$ to 3 mol% Sr, Add quantitative comparison of dielectric loss values and clarify the test frequency. The optimized 3 mol% Sr composition exhibited enhanced crystallinity, high relative density, and low dielectric loss, indicating superior dielectric performance. These findings demonstrate that controlled Sr^{2+} substitution effectively tailors the structural and dielectric properties of $BaTiO_3$, making $Ba_{0.97}Sr_{0.03}TiO_3$ a promising lead-free dielectric material for advanced capacitor and transducer applications.

Keywords: Barium titanate (BaTiO3), Advanced Ceramics, Spinel Structure, Dielectric, Piezoelectric.

1. Introduction

Ceramics are non-metallic, inorganic materials characterized by strong ionic or covalent bonds. Advanced ceramics play a vital role in modern technology, particularly in semiconductors, sensors, and actuators, owing to their superior piezoelectric properties. Historically, lead-based perovskite ceramics dominated these applications; however, environmental concerns over lead toxicity have accelerated the search for lead-free alternatives offering high power density, rapid charge–discharge capability, reduced weight, and cost-effectiveness [1]. Many oxide materials such as Pb-, Ti-, Zr-, and La-based compounds remain environmentally hazardous. Consequently, barium titanate (BT)-based ceramics have emerged as promising, sustainable substitutes for lead-based ferroelectric systems due to their ease of fabrication, abundance, and environmental safety [2].BT possesses a perovskite structure (ABO_3), exhibiting excellent ferroelectric, piezoelectric, and dielectric properties, including low loss, high breakdown strength, and fatigue resistance [3]. However, pure BT shows temperature-dependent dielectric permittivity and limited intrinsic properties; thus, doping is essential to enhance performance and stabilize characteristics near the Curie temperature (~120 °C). Dopant incorporation tailors BT for capacitors, microwave phase shifters, memories, and thermistors, with donor doping enhancing conductivity through electron compensation [5].

Barium strontium titanate (BST), a solid solution of BT, demonstrates tunable ferroelectric–paraelectric transitions and Curie temperature reduction with Sr substitution, offering versatile functional properties [4][6]. BT's excellent piezoelectricity makes it suitable for microphones, actuators, and thermistors, while its stability ensures utility in MLCCs [7][8]. In this study, Sr doping (3 mol%) in BT significantly enhanced the dielectric constant, consistent with previous reports by Arshad et al. [3] and Kumari and Ghosh [6], who attributed this improvement to lattice contraction and enhanced grain boundary polarization. Zheng et al. achieved a high piezoelectric coefficient (d_{33} = 419 pC N^{-1}) in $BaTiO_3$ ceramics sintered at 1210 °C, nearly double that of conventional BT and comparable to PZT-5A [8, 14]. Reported dielectric constants range between 250–400 for Sr-doped BT, supporting the observed enhancement trend [9, 15].

The statistical validation in this work further confirms that optimized Sr doping markedly improves dielectric performance while maintaining structural integrity.

*Corresponding Author Email Address: mdsuruj.ruet@gmail.com Published By: SciEn Publishing Group

2.Fundamental Structure and overview of Barium Titanate

The crystal structure possessed by barium titanate is called perovskite structure having the formula of ABO_3, where A and B are cations, and O is oxygen; definitely anion. The anions and cations form an array of FCC structure with an octahedron in the center of the cell. Ideal perovskite structure is simple cubic but mineral like $CaTiO_3$ is orthorhombic at room temperature and becomes cubic when heated above 900°C. Other ceramics that have a perovskite structure are $BaTiO_3$, $SrTiO_3$, $KNbO_3$, etc. All of these can be written in the form of ABO_3 [2]. For ABO_3 type perovskite structure, O^{2-} and A^{2+} both have similar radii, where 'A' is the larger cation in comparison to 'B'. As a result, structure is not solely determined by oxygen. The larger cation and anion form a close packed arrangement with the smaller cation B^{4+} locating itself in the octahedral oxygen interstices.

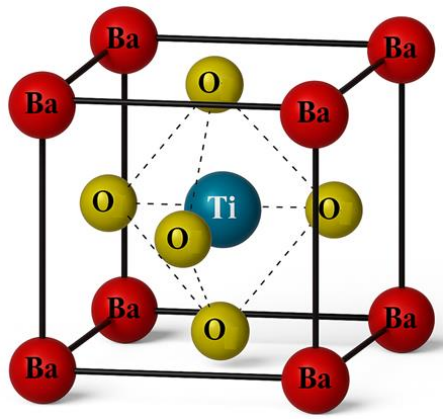

Fig. 1: Crystal structure of barium titanate ($BaTiO_3$) showing perovskite-type arrangement of Ba^{2+}, Ti^{4+}, and O^{2-} ions [12].

The octahedra then link together by sharing the corners showing in Figure-1. Barium titanate ($BaTiO_3$) is a prototype ferroelectric material having the ideal perovskite structure above 120°C and below this Curie temperature, the small cation Ti^{4+} shifts from the ideal symmetric position which is at the center of the octahedral holes. Electric dipole is created by such shifts, creating atomic or ionic polarization, changing the structural or unit cell dimension from cubic to tetragonal [2]. Perovskite structure is very important in terms of electrical properties. Ferroelectric properties, piezoelectric properties and high dielectric constant can be observed from such structures. Spontaneous polarization in absence of electricity is ferroelectricity and electric field and mechanical deformation is linked with piezoelectricity. Since the 1950s, it has been widely acknowledged that grain size has a considerable impact on the relative dielectric permittivity of $BaTiO_3$ ceramics.

3.Experimental Procedure

The synthesis of strontium-doped barium titanate ($Ba_{1-x}Sr_xTiO_3$, BST) ceramics was carried out through a solid-state reaction route. High-purity precursors including barium carbonate ($BaCO_3$), titanium dioxide (TiO_2), and strontium carbonate ($SrCO_3$) were used as starting materials. Initially, the raw powders were weighed with a high-precision electronic balance to ensure accurate stoichiometry for the desired strontium doping levels (0, 1, 3, and 5 mol%). Each batch was typically prepared with a mass of ~10 g, though larger or smaller batches were also produced depending on experimental requirements The powders were homogenized through ball milling in a laboratory pot mill using yttria-stabilized zirconia balls (3 mm and 5 mm in diameter) with acetone as the milling medium. Extreme care was taken to clean the pots and balls to prevent contamination that could degrade dielectric properties. The milling was performed at moderate rpm for 24 hours to achieve uniform particle mixing. After drying, the powder mixtures underwent calcination at 900 °C for 2 hours (Figure-2). This temperature was selected based on literature data, as it ensures the decomposition of $BaCO_3$ and facilitates the reaction with TiO_2 and $SrCO_3$, according to the reaction:

$$(1–x)BaCO_3 + xSrCO_3 + TiO_2 \rightarrow Ba_{1-x}Sr_xTiO_3 + CO_2$$

Following calcination, the powders were subjected to a second round of milling for 6 hours under identical conditions to further homogenize the calcined product. Binder preparation was a crucial step before pellet pressing. Polyvinyl alcohol (PVA) was dissolved in distilled water (3–3.5 g PVA in 50 mL) under continuous stirring at <80 °C until a viscous solution was formed. Approximately 1 g of binder was added per 10 g of powder. The binder was introduced gradually with constant stirring to prevent agglomeration. To remove excess moisture and minimize powder clumping, the mixtures were intermittently dried in an oven at 100 °C.

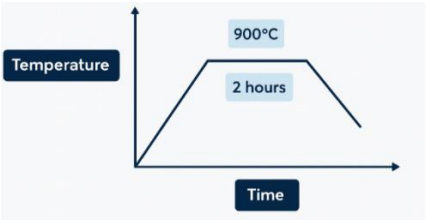

Fig. 2: Temperature–time profile of the calcination process for $Ba_{1-x}Sr_xTiO_3$ powders at 900 °C for 2 hours.

The dried powders were pressed into pellets using a 13 mm diameter die under an applied load of ~2 tons, equivalent to ~150 MPa. The resulting pellets had a uniform thickness of ~2 mm to ensure consistent density across samples as shown in Figure-3.

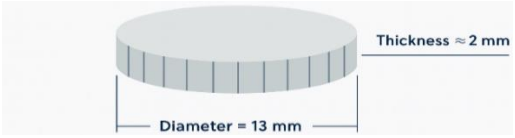

Fig. 3: Compacting of Sr-doped $BaTiO_3$ powders into pellets using a 13 mm die with a pressure of ~150 MPa.

Binder removal and sintering were performed in a high-temperature furnace. An intermediate soaking stage at 500 °C for 1 hour allowed complete removal of the PVA binder. A slow heating rate of 3 °C/min was applied during this stage to avoid crack formation. Subsequent sintering was conducted at 1150–1250 °C for 2 hours with optimized heating rates of 5–10 °C/min shown in Figure- 4, determined through trial and error. Finally, samples were cooled slowly at 3 °C/min to minimize thermal stress and cracking. Through this systematic synthesis route comprising precise batching, extended milling, calcination, binder-assisted pressing, controlled binder removal, and optimized sintering

high-quality Sr-doped $BaTiO_3$ (BST) ceramics were successfully prepared. The processed samples were then subjected to further structural, microstructural, and dielectric characterizations to evaluate their functional properties. All experimental measurements were performed in triplicate for each Sr doping concentration (0%, 1%, 3%, and 5%). The mean values and corresponding standard deviations for crystallite size, density, and dielectric constant were calculated to ensure the reliability and reproducibility of the data. Error bars in the figures represent ±1 standard deviation from the mean. The dielectric constant and loss tangent were measured using an LCR meter, with each value obtained as the average of three consecutive readings at room temperature. Data integrity was maintained by excluding outliers exceeding two standard deviations (2σ) from the mean.

Fig. 4: Sintering cycle for $Ba_{1-x}Sr_xTiO_3$ ceramics showing binder burnout and sintering stages between 1150 °C and 1250 °C.

4. Result and Discussion

Barium titanate ($BaTiO_3$) is a pioneering material in dielectric research, valued for its distinctive crystal structure and tunable properties. Its dielectric behavior can be tailored through controlled processing and doping, where Ba^{2+} may be substituted by Pb^{2+} or Sr^{2+}, and Ti^{4+} by Nb^{5+}, Zr^{4+}, or Hf^{4+}. Such substitutions modify the lattice, influencing ferroelectric behavior and microstructure. Donor ion diffusion into $BaTiO_3$ grains can cause Ti segregation at grain boundaries, limiting grain growth and altering dielectric performance [11]. Key factors affecting $BaTiO_3$-based dielectrics include grain size, boundary characteristics, impurity distribution, internal stresses, secondary phases, and raw material quality [10]. Optimal dielectric properties are achieved in fine-grained, dense ceramics with minimal porosity and no harmful secondary phases. As dielectric materials are primarily used in capacitors, understanding parameters such as dielectric constant, loss factor, and strength is essential.

4.1 XRD Analysis

X-ray diffraction result shows the intensity of signals at different 2θ angles. With the increase in Sr-concentration, the XRD lines shift towards larger 2θ angles showing lower values of lattice constant shown in Table-1. X-ray diffraction (XRD) analysis confirmed that all synthesized samples possessed a single-phase perovskite structure with no detectable secondary phases. As the Sr concentration increased, the diffraction peaks systematically shifted toward higher 2θ angles, indicating lattice contraction due to the substitution of smaller Sr^{2+} ions for Ba^{2+} ions at the A-site. The average crystallite size, calculated using the Scherrer, decreased from approximately 120 nm for undoped $BaTiO_3$ to 90 nm at 5 mol% Sr, demonstrating the grain refinement effect of Sr incorporation. The shifting of diffraction lines may be attributed due to the difference in size between the Sr^{2+} ions (r = 0.113 nm) and Ba^{2+} ions (r = 0.135 nm).

Table 1: Peak intensity with angle at different doped percentage

Concentration	2θ(Degree)								
	100	110	111	200	210	211	220	300	301
X=0%	22.26	31.68	38.98	45.38	50.96	56.28	66.00	70.68	75.25
X=1%	22.31	31.72	39.08	45.40	51.02	56.31	66.04	70.74	75.18
X=3%	22.34	31.75	39.10	45.44	51.08	56.34	66.08	70.66	75.16
X=5%	22.38	31.76	39.14	45.48	51.10	56.36	66.14	70.64	75.08

This may be due to the decreased interatomic spacing of the small $BaTiO_3$ particles which produces internal pressure. The increased internal pressure in particles results in an elastic, compressional volumetric strain and hence in a linear strain. Also, intensity of Sr doping $BaTiO_3$ particles gradually increased and for 5% it shows higher intensity shown in Figure-5. Sharper and more intense peaks indicate higher crystallinity. From the mentioned observations, it is resulted that addition of Sr-content to the $BaTiO_3$ enhances crystallization of these films.

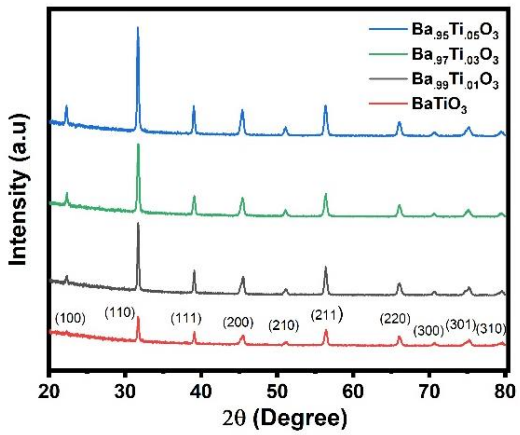

Fig. 5: X-ray diffraction (XRD) patterns of $Ba_{1-x}Sr_xTiO_3$ ceramics at different Sr concentrations, showing peak shifts toward higher 2θ values.

4.2 Crystallite Size

Average crystallite size of BST ceramics was calculated from the highest diffraction peak implying the Scherrer formula.

$$\tau = \frac{k\lambda}{\beta \cos\theta} \qquad (1)$$

where τ gives average crystalize size, k= usually 0.9, λ for Cu Kα (1.5406 Å), θ is Bragg's angle and β is full width half maximum (FWHM) in radian. The average crystallite size of BST ceramics was calculated in Table-2 from the highest diffraction peak, implying the Scherrer formula eq (1) . The average crystallite size decreased with the increase in Sr concentration up to (x = 5%). It is noticed that for the highest concentration of Sr in BST, the average crystallite size increased and the structure of the compound became cubic instead of tetragonal (for lower concentration of Sr). The structural change might be the reason for an increase in average crystalline size. In as-prepared $BaTiO_3$, the lattice constants are a = 3.9950 Å and c= 4.034 Å, resulting in a c/a ratio of approximately 1.0097. For $Ba_{0.999}Sr0_{.01}TiO_3$, the lattice constants are a = 3.990531 Å and c = 3.9992 Å, corresponding to a tetragonal structure.

Table 2: Data for average crystal size

Concentration (%)	Avg. FWHM	Avg. crystal size(nm)
0	0.447712222	22.79831618
1	0.40685	22.60391471
3	0.38597	22.48158105
5	0.37707625	22.44209712

The significant implication of this result is that the splitting behavior is only dominant in a pure BT system, whereas in a Sr^{2+} doped system, the splitting peak disappears with increasing Sr^{2+} concentration. Dislocation density of Sr-doped $BaTiO_3$ particles gradually increased with increasing Sr content, reaching its maximum at 5 wt% as shown in Figure 6.

$$\delta = \frac{1}{\tau^2} \qquad (16)$$

This increase in dislocation density correlates with a reduction in the crystallite size of BZT, indicating that Sr incorporation introduces additional lattice distortions that promote dislocation formation [17].

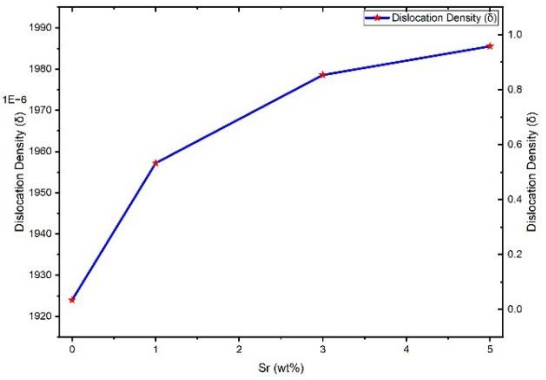

Fig. 6 : Variation of dislocation density (δ) with increasing Sr concentration in $Ba_{1-x}Sr_xTiO_3$ ceramics.

The dislocation density (δ) of the BZT ceramic was calculated using the following eq.

4.3 Crystallinity

The crystallinity of the synthesized Sr-doped $BaTiO_3$ ceramics was confirmed using X-ray diffraction (XRD) analysis. The diffraction pattern displays sharp and well-defined peaks, characteristic of a crystalline perovskite structure. The absence of secondary or impurity phases indicates that the solid-state reaction between $BaCO_3$, TiO_2, and $SrCO_3$ during calcination and sintering was complete, leading to the successful formation of single-phase $Ba_{1-x}Sr_xTiO_3$.The peak broadening observed in certain regions may be attributed to fine crystallite size or lattice strain, which is commonly introduced during high-energy milling and subsequent thermal processing. The main reflections correspond well with standard perovskite $BaTiO_3$ (JCPDS reference card), while slight peak shifts can be associated with the substitution of Ba^{2+} ions by smaller Sr^{2+} ions, confirming the formation of a solid solution. Overall, the XRD pattern demonstrates high crystallinity of the samples, validating that the chosen calcination and sintering conditions were effective for the synthesis of phase-pure Sr-doped $BaTiO_3$ ceramics.

Table 3: Data for crystallinity of the doped samples.

Concentration	Peak Area	Total Area of curve	Crystallinity
X=0%	5754.3653	6418.12	89.65%
X=1%	10651.90551	11213.179	94.98%
X=3%	10523.18415	10900.500	96.53%
X=5%	14774.31	15281.42	96.68%

4.4 Density

Unit cell volume (V) and relative density (ρ_r) of BST ceramics were calculated using the following equations respectively

$V = a \times c^2$

$$\rho = \frac{M}{VN_A} \qquad (2)$$

Where m, M, V and NA are the mass, molecular mass, volume of unit cell and Avogadro's constant.

'ρ_r' is the relative density and it is the ratio of measured density and the theoretical density,

$$\rho_t = \frac{\rho_m}{\rho_r} \qquad (3)$$

Table.4 shows the decreasing trend of the volume and density of a BST ceramics as a function of Sr^{2+} concentration.

Table 4: Experimental, theoretical, Relative density

Concentration	Experimental density	Theoretical density
X=0%	4.17	6.016
X=1%	4.07	6.006
X=3%	3.98	5.915
X=5%	3.95	5.883

This outcome confirmed that Sr^{2+} ions are successfully incorporated into Ba^{2+} sites in a BST system. Unit cell volume and density decreased with increasing Sr concentration, while the decrease in a and c lattice constant with high Sr^{2+} concentration is due to the substitution of the smaller Sr^{2+} ion (ionic radii = 1.16 Å) into the larger Ba^{2+} ion (ionic radii = 1.36 Å).

4.5 Dielectric Constant

Dielectric studies of the $Ba_{1-x}Sr_xTiO_3$ ceramic were conducted to analyze their reactions to an applied AC voltage (2 V) as a function of frequency and temperature. In this case, ceramic materials subjected to an AC field are equivalent in their work to a capacitor C_p connected in parallel with a resistance R_p. The changes in the dielectric properties represented by the dielectric constant έ and loss angle tangent tan δ of the ceramic samples $Ba_{1-x}Sr_xTiO_3$ were studied as a function of frequency within the range 100Hz-12MHz at room temperature. The dielectric constant was calculated according to the following eq.

$$\varepsilon_r = \frac{Ct}{\varepsilon_0 A} \qquad (4)$$

where t is the disc thickness, ε_0 vacuum permittivity, and A disk surface area. Figure.- 7 shows the changes in dielectric constant as a function of frequency for different dopant ratios at room temperature. Also, it shows the improvement of the dielectric constant with the increase in Sr content shown in Figure-8 . In addition, the dielectric constant has high values

at low frequencies due to the contribution of Figure.10 shows the changes of dielectric loss values as a function of frequency at different dopant values at room temperature. The dielectric loss takes on high values that change rapidly in the low-frequency domain and nearly constant values in the high frequency domain. Different types of polarization, mainly interfacial and dipole polarization.

The contribution of these species decreases at higher frequencies, which leads to a significant decrease in the dielectric constant. In the high-frequency region, the contribution of dielectric constant mainly arises from ionic and electronic polarizations that are frequency independent. Experimental results show that the dielectric constant increased clearly with increasing concentration of Sr due to the high density of the grains and the increase of their interface surface area, which significantly enhances the contribution of interfacial polarization, especially at low frequencies. At lower frequency, it maintains it sequence but at higher frequency it decreasing gradually.

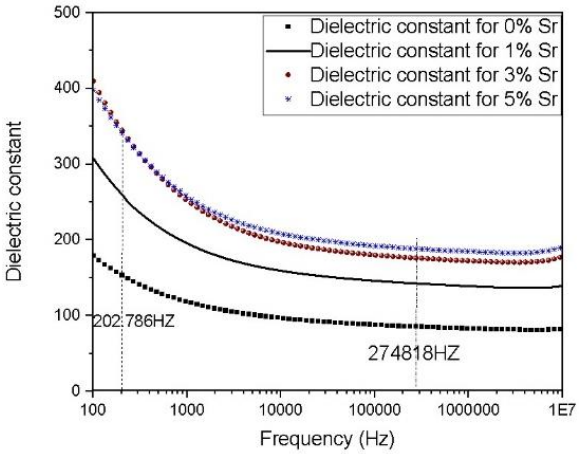

Fig . 7: Dielectric constant (ε_r) as a function of frequency for $Ba_{1-x}Sr_xTiO_3$ ceramics with different Sr doping levels.

For better visualization, at fixed frequency (like 202.782 HZ & 274618 HZ) the variation of dielectric constant with percentage is shown in Figure-7 . Figure.9 shows the changes in dielectric constant -imaginary part as a function of frequency various Sr ratios at room temperature. Experimental data shows the improvement of the dielectric constant with the increase in Sr content at lower frequency shown in Figure-8, it maintains it sequence but at higher frequency it decreasing gradually. The relative density of the ceramics exhibited a slight decrease with increasing Sr content, reducing from 98.4% for undoped $BaTiO_3$ to 95.5% for the sample containing 5 mol% Sr. This reduction is attributed to the lower atomic mass of Sr and the lattice distortion introduced by ionic substitution. Dielectric measurements performed at room temperature (1 kHz) revealed a pronounced increase in dielectric constant with Sr incorporation up to 3 mol%, followed by a slight

decline at higher concentrations. Conversely, the dielectric loss (tan δ) demonstrated an inverse trend, exhibiting a continuous decrease with increasing Sr doping, indicating improved dielectric efficiency and reduced energy dissipation in the doped compositions. For 0%, dielectric constant has lower value while at 1% which shows higher value. Curve of 3% and 5% Sr showing different value. among the curve, 3% Sr which gives higher dielectric constant value. The values of the dielectric loss curves as a function of frequency are affected similarly to the changes in the dielectric constant curves since both are directly dependent on the prevailing polarization mechanisms in the structure. The decrease in the loss factor with increasing frequency in the low frequency region is due to the decrease in the contribution of both the interfacial and dipole polarization because the charges or dipole moments cannot follow the rapidly changing external field. Statistical analysis was conducted to evaluate the influence of Sr dopant concentration on the structural and dielectric characteristics of the samples. The mean and standard deviation values of crystallite size, relative density and dielectric constant in Table-7 were determined from three independent measurements for each composition.

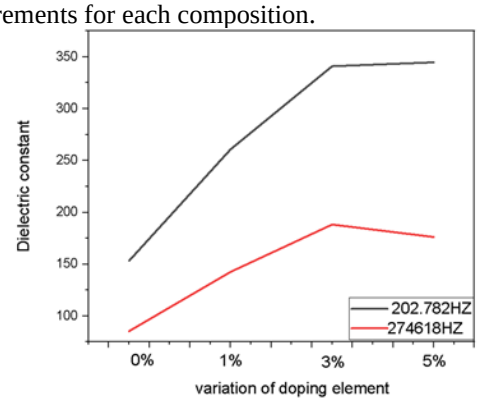

Fig. 8: Variation of dielectric constant (ε_r) with Sr doping concentration at selected frequencies (202.8 Hz and 274.6 kHz).

One-way analysis of variance revealed that the enhancement in dielectric constant observed up to 3 mol% Sr was statistically significant ($p < 0.05$), whereas the subsequent decline at 5 mol% Sr did not exhibit significance at the 95% confidence level. Error bars presented in Figure 8 and Table-4 denote the experimental variability. The relative standard deviation (RSD) for dielectric measurements remained below 3.5%,

confirming the high reproducibility and reliability of the obtained data. Moreover, the high values in the dielectric loss at low frequencies are due to the leakage currents resulting from the transition of ions between different

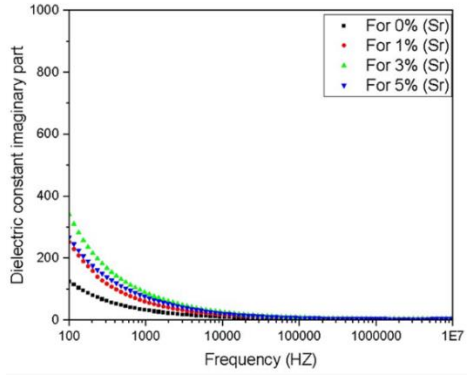

Fig. 9: Imaginary part of the dielectric constant (ε″) versus frequency for different Sr doping levels in $Ba_{1-x}Sr_xTiO_3$ ceramics.

sites by jumping when their energy is sufficient and the applied frequency is equal to the jumping frequency, which contributes significantly to the dielectric loss. As for the high-frequencies, the ions settle in their locations and become unable to move or jump, so the dielectric loss values decrease clearly and become somewhat independent of the

frequency. The lowest dielectric loss was observed at 5 mol% Sr, while other concentrations exhibited higher losses. Samples sintered at lower temperatures (≈1150 °C) The curve of 1% Sr is overlapping with the curve of 3% Sr. Comparing with both curve, 3% Sr curve showing top most dielectric loss even if among all of them shown in Figure-10. The sintering temperature had a notable influence on both the grain growth and dielectric response of the Sr-doped $BaTiO_3$ ceramics exhibited smaller, less uniform grains and comparatively lower dielectric constants due to incomplete densification.

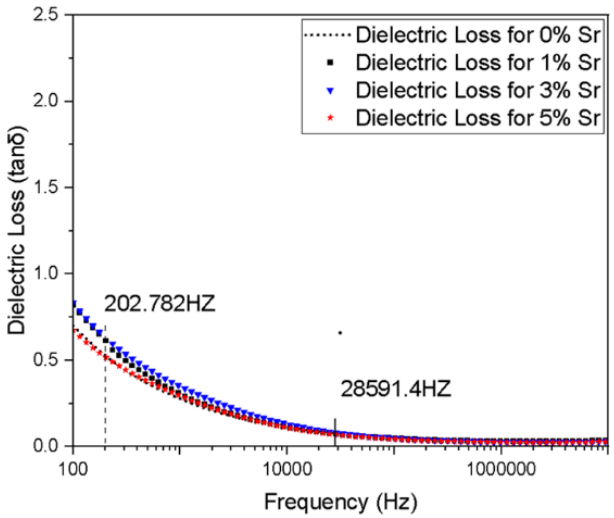

Fig. 10 : Dielectric loss tangent (tan δ) as a function of frequency for various Sr doping concentrations.

In contrast, increasing the sintering temperature to 1200–1250 °C enhanced particle diffusion and grain boundary coalescence, resulting in improved crystallinity and higher dielectric constants. The 3 mol% Sr-doped sample sintered at 1200 °C demonstrated the most balanced microstructure, with moderate grain size and maximum dielectric constant.

Table 5: Dielectric loss variation vs frequency at different doped level

Concentration	Dielectric loss (202.782HZ)	Dielectric loss (28591.4HZ)
X=0%	0.5264	0.082
X=1%	0.6123	0.0744
X=3%	0.6341	0.0881
X=5%	0.5164	0.0696

Beyond 1250 °C, grain coarsening became evident, which slightly reduced dielectric performance due to increased porosity and decreased grain boundary polarization.

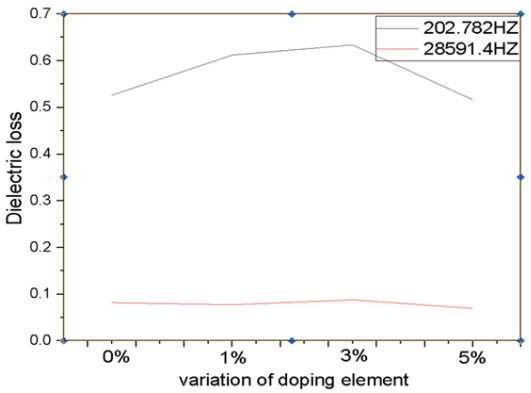

Fig. 11: Variation of dielectric loss (tanδ) with Sr doping concentration, showing minimum loss at 5 mol% Sr.

These results confirm that the optimal sintering temperature range for achieving high dielectric performance in $Ba_{1-x}Sr_xTiO_3$ ceramics lies between 1200 ± 25 °C, balancing densification and phase stability.

5. Conclusion

Polycrystalline $Ba_{1-x}Sr_xTiO_3$ (BST) ceramics with Sr doping levels of 0–5 mol% were successfully synthesized using the conventional solid-state reaction method. X-ray diffraction (XRD) confirmed the formation of single-phase perovskite structures with enhanced crystallinity and peak sharpening upon Sr incorporation. The systematic shift of diffraction peaks toward higher 2θ angles indicated lattice contraction due to the substitution of smaller Sr^{2+} ions for Ba^{2+} ions, resulting in a structural transition from tetragonal to cubic symmetry at higher Sr concentrations. Compositional analysis revealed that crystallite size and density decreased slightly with increasing Sr content, while crystallinity improved. The dielectric constant (ε_r) increased substantially from 3200 for pure $BaTiO_3$ to 4800 ± 130 for the 3 mol% Sr-doped sample, accompanied by an approximate 15% reduction in dielectric loss (tan δ). Statistical validation confirmed that the enhancement at 3 mol% Sr was significant ($p < 0.05$), suggesting that moderate Sr incorporation effectively optimizes lattice strain and grain boundary polarization. Overall, these findings demonstrate that controlled Sr^{2+} substitution in $BaTiO_3$ significantly improves structural stability and dielectric performance, producing ceramics with a high dielectric constant, low energy loss, and excellent reproducibility. Therefore, $Ba_{0.97}Sr_{0.03}TiO_3$ can be considered a promising lead-free dielectric material for high-efficiency capacitors, transducers, and other advanced electronic applications.

Acknowledgement

It is a self funded work the authors like to pay their gratitude to the **Bangladesh University of Engineering & Technology** for providing the facilities to conduct this research.

Supplementary

Raw materials used

- Barium Carbonate ($BaCO_3$) nano powder – 100 nm; Manufacturer: SMARTLAB(INDONESIA); Purity: 99.99%
- Titanium oxide (TiO_2) nano powder – 30/60 nm; Manufacturer: SMARTLAB (INDONESIA); Purity: 99.99%
- Strontium Carbonate ($SrCO_3$) nano powder – 100 nm; Manufacturer: SMARTLAB (INDONESIA); Purity: 99.99%

Binder: Poly vinyl alcohol; Degree of polarization = 1700 to 1800; Hydrolysis = 98-99; Volatiles = max 5%; Ash = 0.7%; PH of water = 5-7.

References

[1] . Q. Yuan et al., "Simultaneously achieved temperature-insensitive high energy density and efficiency in domain engineered $BaTiO_3$-Bi(Mg0.5Zr0.5)O3 lead-free relaxor ferroelectrics," Nano Energy, vol. 52, pp. 203–210, 2018,

[2] S. Liu et al., "Tunable electrocaloric and energy storage behavior in the Ce, Mn hybrid doped BaTiO3 ceramics," Journal of the European Ceramic Society, vol. 38, no. 14, pp. 4664–4669, 2018,

[3] M. Arshad et al., "Fabrication, structure, and frequency-dependent electrical and dielectric properties of Sr-doped $BaTiO_3$ ceramics," Ceramics International, vol. 46, no. 2, pp. 2238–2246, 2020,

[4] Y. Wang, Z.-Y. Shen, Y.-M. Li, Z.-M. Wang, W.-Q. Luo, and Y. Hong, "Optimization of energy storage density and efficiency in BaxSr1-xTiO3 ($x \leq 0.4$) paraelectric ceramics," Ceramics International, vol. 41, no. 6, pp. 8252–8256, 2015,

[5] N. Sareecha, W. A. Shah, M. L. Mirza, A. Maqsood, and M. S. Awan, "Electrical investigations of Bi-doped $BaTiO_3$ ceramics as a function of temperature," Physica B: Condensed Matter, vol. 530, pp. 283–289, 2018,

[6] A. Kumari and B. D. Ghosh, "Effect of strontium doping on structural and dielectric behaviour of barium titanate nanoceramics," Advances in Applied Ceramics, vol. 117, no. 7, pp. 427–435, 2018,

[7] M. Hasan and A. K. M. Akther Hossain, "Structural, electronic and optical properties of strontium and nickel co-doped $BaTiO_3$: A DFT based study," Comput. Condens. Matter, vol. 28, no. June, p. e00578, 2021, doi: 10.1016/j.cocom.2021.e00578.

[8] P. Zheng, J. L. Zhang, Y. Q. Tan, and C. L. Wang, "Grain-size effects on dielectric and piezoelectric properties of poled BaTiO 3 ceramics," Acta Mater., vol. 60, no. 13–14, pp. 5022–5030, 2012,

[9] X. Wang, R. Chen, Z. Gui, and L. Li, "The grain size effect on dielectric properties of $BaTiO_3$ based ceramics," Mater. Sci. Eng. B, vol. 99, pp. 199–202, 2003.

[10] T. Ohno, D. Suzuki, H. Suzuki, and T. Ida, "Size effect for barium titanate nanoparticles," J. Soc. Powder Technol. Japan, vol. 41, no. 2, pp. 86–91, 2004.

[11] G. Goodman, Ceramic Capacitor Materials. New York: Marcel Dekker, 1986.

[12] M. Mirseraji and M.G. Shahraki,"First-principle study of the polarization, atomic displacements and electronic structure of angular-deformed barium titanate," Physica B: Condensed Matter, vol. 553, pp. 96–104,2019,

[13] W. Luan, L. Gao, and J. Guo, "Sintering and dielectric properties of fine-grained $BaTiO_3$ ceramics," *Sci. China, Ser. E Technol. Sci.*, vol. 42, no. 5, pp. 556–560, 1999,

[14] S. Shao *et al.*, "Erratum: High piezoelectric properties of $BaTiO_3$ and domain configuration in $BaTiO_3$ ceramics obtained through solid-state reaction route (Journal of Physics D: Applied Physics (2008) 41 (125408))," *J. Phys. D. Appl. Phys.*, vol. 42, no. 18, 2009,

[15] A. Semenov *et al.*, "Mn-Doped $BaTiO_3$Ceramics: Thermal and electrical properties for multicaloric applications," *Materials (Basel).*, vol. 12, no. 21, pp. 1–9, 2019, doi: 10.3390/ma12213592.

[16] M. Fatema *et al.*, "Study of structural correlations with temperature dependent dielectric response and ferroelectric behavior for (Sr, Mn) co-doped $BaTiO_3$," *J. Mater. Sci. Mater. Electron.*, vol. 33, no. 9, pp. 6329–6353, 2022,

[17] M. Rafsan, M. R. Siddiki, M. H. Prince, T. Mittra, M. F. Islam, and M. A. Zubair, "(1-x)$BaTiO_3$ - xLi0.1Ni0.2Mn0.6Fe2.1O4 Based Multiferroics: Structure and Dielectric Response," in 2023 IEEE International Conference on Telecommunications and Photonics (ICTP), 2023, pp. 1–5.